EXTRACTION OF REGION BOUNDARY PATTERNS WITH ACTIVE CONTOURS

Mohamed Ben Salah[1] and Amar Mitiche[2]
[1]*Department of Computing Science, University of Alberta, Edmonton, AB, Canada*
[2]*Institut National de la Recherche Scientifique, Montreal, QC, Canada*

Keywords: Image Segmentation, Boundary Features, Distributions Matching, Active Curves, Level Sets.

Abstract: In this study we address the problem of recovering region boundary patterns consistent with a given pattern. A level set method formulated in the variational framework evolves an active contour towards regions of interest boundaries while omitting the others. The curve evolution results from the minimization of a functional which measures the similarity between the distribution of an image-based geometric feature on the curve and a model distribution. The corresponding curve evolution equation can be viewed as a geodesic active contour flow having a variable stopping function. This affords a global representation of the objects boundaries which can effectively drive active curve segmentation in a variety of otherwise adverse conditions. We ran several experiments supported by quantitative performance evaluations using various examples of segmentation and tracking.

1 INTRODUCTION

Image segmentation is a central problem and extensively researched topic in computer vision. It serves numerous applications such as medical image analysis, robotics, surveillance, and remote sensing (Holtzman-Gazit et al., 2006; Ben Ayed et al., 2005; Mortensen, 2008).

Leading to the most effective, numerically efficient and stable algorithms, the active contour variational formulations are widely adopted in a variety of settings (Chan and Vese, 2001; Cremers et al., 2007; Freedman and Zhang, 2004; Ben Ayed et al., 2009; Paragios and Deriche, 2002). The problem is formulated as a minimization problem of an objective functional which embeds the constraints on the segmentation. The ensuing Euler-Lagrange equations, minimizing the objective functional, are evolution equations which drive the active contours towards the relevant region boundaries. The objective functional data terms, which measure the conformity of the image to model descriptions, are either edge-based when they evaluate an image function along the active curve, or region-based when they refer to the image within the region enclosed by the curve. Therefore, the corresponding curve evolution velocities are due to the image exclusively along or within the curve.

Edge-based methods have been among the first active contour solutions proposed for image segmentation problems. The Snake model (Kass et al., 1988), and the geodesic active contour (GAC) which adopted a more effective curve representation (Caselles et al., 1997), were precursory of a vast literature on edge-based active curve image segmentation (Kass et al., 1988; Caselles et al., 1997; Paragios et al., 2004; Kichenassamy et al., 1995; Paragios and Deriche, 2002). Typically, these algorithms attract the active curve toward high contrast boundaries of the image, which are assumed to coincide with desired regions boundaries, by minimizing a geodesic integral along the contour of a decreasing function of the image gradient. In general, geodesics are seriously challenged when the desired boundaries have segments of low gradient or when all the objects, the desired and non desired objects, present high image transitions ans similar intensity profiles. For instance, in magnetic resonance imaging (MRI) and computed tomography (CT) medical images, the organs of interest can present very weak edges and high intensity similarity with neighboring structures. In such cases, the geodesic contours leak away from the desired boundaries and may vanish.

Region-based schemes, which refer to the image over regions, were later proposed to overcome these kind of problems. In region-based algorithms, each segmentation region is characterized by an image dis-

Ben Salah M. and Mitiche A..
EXTRACTION OF REGION BOUNDARY PATTERNS WITH ACTIVE CONTOURS.
DOI: 10.5220/0003826102400248
In *Proceedings of the International Conference on Computer Vision Theory and Applications* (VISAPP-2012), pages 240-248
ISBN: 978-989-8565-03-7

tribution, i.e., the regions are assumed to differ by their image statistics. Hence, they are significantly less sensitive to weak boundary gradient than the geodesic schemes (Chan and Vese, 2001; Zhu and Yuille, 1996; Samson et al., 2000; Ben Ayed et al., 2005). Following the seminal work of Chan and Vese (Chan and Vese, 2001) which uses region means, various algorithms have been proposed. In general, they use a global model description of the image within the extent of each desired region to penalize movements of the active curves in or out of the regions they are intended to delineate. Both parametric (Chan and Vese, 2001; Mansouri et al., 2006; Ben Ayed et al., 2006; Salah et al., 2010) and non-parametric (Freedman and Zhang, 2004; Rousson and Cremers, 2005; Michailovich et al., 2007) image descriptions have been used for the purpose. However, and in spite of this accrued robustness, the region-based active curve evolution can be seriously challenged, by definition, when the regions to segment have similarly distributed segments (Ben Ayed et al., 2009). When these segments occur between regions, the placement of the separating boundary becomes largely ambiguous.

Other methods combine the advantages of both edge-based and region-based models in order to overcome the mentioned problems (Paragios and Deriche, 2002; Vazquez et al., 2006). However, current methods are still not applicable especially when the target regions are rather characterized by the distribution of a feature on their boundary. In other words, this happens when region boundaries are considered patterns described by a geometric feature distribution rather than simply the location of the feature as with typical geodesic descriptions. One typical example where this description of boundaries by a geometric feature distribution is befitting is depicted in Figure 1. This example is of an image where regions occur with boundaries that are either rectangular or ellipsoidal outline. For each outline pattern there are two regions of varying appearance and the goal of segmentation is to extract, in a single instantiation, the regions of each of the two patterns. Matching the distribution of *boundary curvature*, measured from the image gradient, against a model distribution, has extracted both rectangular regions in one case (Figure 1 (a)) and both ellipsoidal regions in the other (Figure 1 (b)), without prior knowledge of the number of regions. Note that a shape prior constraint will not be able to segment all of the regions of the same figure, unless one such prior is used for each region, and each with an accompanying close by initialization, which supposes an information about the image not available for practical purposes, such as the number of objects as well as the

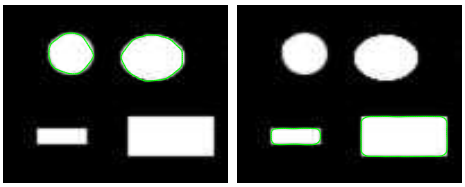

(a) (b)

Figure 1: The segmentation targets elliptical objects in (a) and rectangular objects in (b). Only the targeted objects should be segmented.

section of the image domain where each occurs (Cremers et al., 2003; Chan and Zhu, 2005). Because, a shape prior is an image-independent term added to the segmentation functional so as to bias a detected region to have a given geometric outline modulo a transformation (such as rigid or affine) (Cremers et al., 2007; Leventon et al., 2000; Cremers et al., 2006), a shape prior constraint will also require additional optimization over pose transformations, or a constraint on the curve deformation with respect to a reference shape (Foulonneau et al., 2006; Foulonneau et al., 2009).

The purpose of this study is to take full advantage of the statistical image information that one can learn about the boundary of interest. We investigate a level set variational segmentation method which drives an active curve to coincide with boundaries on which a geometric feature distribution matches a reference distribution. Indeed, we propose to minimize a contour-based functional which measures the similarity between the distribution of an *image-based geometric feature* along the curve and a reference distribution learned a priori. The scheme is formulated using the Kullback-Leibler similarity measure and is applied to simultaneously recover all region boundaries consistent with a given outline pattern using the isophote curvature as the geometric feature. Note that other features can be used such as the differences of curvatures and angle tangents, and also other similarity measures such as the Bhattacharyya measure can be adopted. A detailed experimentation (Section 4) shows that the scheme is valid and can improve on region and edge based methods. Compared to the region-based formulations in (Freedman and Zhang, 2004; Ben Ayed et al., 2009; Michailovich et al., 2007), the objectives of the proposed functionals are fundamentally different. For instance, the formulations in (Freedman and Zhang, 2004; Ben Ayed et al., 2009; Michailovich et al., 2007) would not distinguish, and it is not their purpose, between the elliptical and rectangular regions in Figure 1 (a,b) because these regions have exactly the same image distributions. The marginal similarity with these studies is in using global measures, but the curve evolution

equations we obtained are quite different. Such a difference will be evidenced in the experiments. Minimization of the proposed functional is carried out by deriving Euler-Lagrange equations implemented via level set techniques. Interestingly, each of the evolution equations we obtained can be viewed as a GAC having a variable stopping function. However, the stopping functions have two fundamental differences with the usual GAC stopping function. First, they depend both on the image and the curve, when the GAC stopping function depends only on the image. Second, they reference the curvature distribution along the contour, a global information, rather than just pixel-wise characteristic as with GAC; such a richer information should afford a better boundary detection behavior. An interpretation of this behavior will be discussed later.

2 FORMULATION

2.1 Objective Function

Let $I : \Omega \subset \mathbb{R}^2 \rightarrow \mathbb{R}$ be an image function, $\gamma : [0,1] \rightarrow \Omega$ a simple closed plane parametric curve, and $F : \Omega \subset \mathbb{R}^2 \rightarrow \mathcal{F} \subset \mathbb{R}$ a feature function from the image domain Ω to a feature space $\mathcal{F}$. Let P_γ be a kernel density estimate of the distribution of F along γ,

$$\forall f \in \mathcal{F} \quad P_\gamma(f) = \frac{\oint_\gamma K(f - F_\gamma) ds}{\mathcal{L}_\gamma}, \tag{1}$$

where F_γ is the restriction of F to γ, $\mathcal{L}_\gamma$ is the length of γ given by $\mathcal{L}_\gamma = \oint_\gamma ds$, and K is the estimation kernel. In this work, we consider the Gaussian kernel of width h given by

$$K(z) = \frac{1}{\sqrt{2\pi h^2}}\, exp^{-\frac{z^2}{2h^2}}. \tag{2}$$

Given a model feature distribution $\mathcal{M}$, let $\mathcal{D}(P_\gamma, \mathcal{M})$ be a similarity measure between P_γ and $\mathcal{M}$. The purpose of this work is to determine $\tilde{\gamma}$ such that

$$\tilde{\gamma} = \arg\min_\gamma \mathcal{D}(P_\gamma, \mathcal{M}). \tag{3}$$

To apply this formulation we need to specify the feature function, the model, the similarity, and a scheme to conduct the objective functional minimization in Eq. (3).

2.2 Feature

Various types of image-base features can be employed depending on the segmentation problem at hand. There are two fundamental types of boundary representation features. One type is the *photometric*, where the feature is a function of the image such as image intensity, its gradient, or any scalar image filter output. The other type of feature function is the *geometric*, which pertains to the boundary form, irrespective of the image function. The curvature, which belongs to this category, is the feature adopted in this work. It can be estimated from the image under the assumption that the region boundary normals coincide with the isophote normals:

$$F = \kappa_I = div\left(\frac{\nabla I}{\|\nabla I\|}\right). \tag{4}$$

Studies have shown that curvature histograms, which can be viewed as empirical marginal distributions of the shape considered a random variable, are useful statistics to describe closed regular plane shapes (Zhu, 2003). Ideally, a geometric description is invariant to the shape position, orientation, and size. It must also be robust to the distortions which normally affect the shape. Curvature, which is the rate of change of the tangent angle along the contour (Do Carmo, 1976), is invariant to translation and rotation but varies with scale. However, this variability is taken into account by an affine transformation of the curvature values so that they always correspond to the same set of bins. For practical means, this normalization makes the histograms unaffected by scale.

Geometric features are necessary when the target object boundary has no specific photometric description, either because the description varies with the picture in which the object appears (e.g., as in Fig. 4 where objects can appear with different colors/textures and/or over different backgrounds) or because there are no photometric features which would distinguish the target from other objects in the image (as in Fig. 2).

2.3 Similarity

The Kullback-Leibler divergence is a common similarity function between distributions. Several studies have used it for foreground-background image segmentation (Mitiche and Ayed, 2010). Efficient applications of the Kullback-Leibler divergence have been reported in (Freedman and Zhang, 2004) in active contour segmentation. It has been part of effective image segmentation formulations (Freedman and Zhang, 2004) (Mansouri and Mitiche, 2002) (Myronenko and Song, 2009) (Lecellier et al., 2009). As well, the bhattacharyya coefficient has also been implemented to match the distribution along contours of a local image average to the distribution along a model object boundary (Ben Ayed et al., 2010). Stud-

ies which mention or use both measures have presented them as alternatives.

We implemented the minimization in Eq. 3 for the Kullback-Leibler divergence as the similarity function $\mathcal{D}$. The Kullback-Leibler divergence between P_γ and $\mathcal{M}$ is

$$\mathcal{D}(P_\gamma, \mathcal{M}) = KL(P_\gamma, \mathcal{M}) = \int_{\mathcal{F}} \mathcal{M}(f)\, \log \frac{\mathcal{M}(f)}{P_\gamma(f)}\, df. \tag{5}$$

Higher values of the Kullback-Leibler divergence indicate smaller overlaps between the distributions. The symmetry of the similarity function with respect to its two distribution arguments (the Kullback-Leibler divergence is not symmetric) is not an issue here because we want to asses how close a variable distribution is to a fixed (model) distribution. Next, we derive the Euler-Lagrange descent equations corresponding to Eq. (3) for the Kullback-Leibler similarity.

3 MINIMIZATION

The data term in Eq. (3) is a measure of similarity between distributions over the boundary representation curve γ. We will address this problem by continuous optimization via the associated Euler-Lagrange γ-evolution descent equations. Let γ be embedded in a one-parameter family of curves indexed by (algorithmic) time t:$\gamma(s,t) : [0,1] \times \mathbb{R}^+ \to \Omega$, and deriving the Euler-Lagrange descent equation

$$\frac{\partial \gamma}{\partial t} = -\frac{\partial \mathcal{D}}{\partial \gamma}. \tag{6}$$

For $\mathcal{D}(P_\gamma, \mathcal{M}) = KL(P_\gamma, \mathcal{M})$, we have:

$$\begin{aligned} \frac{\partial \mathcal{D}}{\partial \gamma} &= \frac{\partial KL}{\partial \gamma} = \int_{\mathcal{F}} \mathcal{M}(f)\, \frac{\partial}{\partial \gamma} \log\Big(\frac{\mathcal{M}(f)}{P_\gamma(f)}\Big)\, df \\ &= -\int_{\mathcal{F}} \mathcal{M}(f)\, \frac{\partial}{\partial \gamma} \log\Big(\frac{\oint_\gamma K(f - F_{\gamma(s)})ds}{\mathcal{L}_\gamma}\Big)\, df \\ &\overset{\frac{\partial \mathcal{L}_\gamma}{\mathcal{L}_\gamma \partial \gamma}}{=} -\int_{\mathcal{F}} \mathcal{M}(f)\, \frac{\partial}{\partial \gamma} \log\Big(\oint_\gamma K(f - F_{\gamma(s)})ds\Big)\, df \end{aligned} \tag{7}$$

where, we recall, F_γ is the restriction of F to γ. Both curve length $\mathcal{L}_\gamma$ and the second integral in Eq. 7 can be written as $\oint_\gamma h ds$, where h is a scalar function, and their functional derivative with respect to γ is of the form (Caselles et al., 1997):

$$\frac{\partial \oint_\gamma h ds}{\partial \gamma} = (-h\kappa + \nabla h \cdot \vec{n})\, \vec{n}, \tag{8}$$

where $\vec{n}$ is the inward unit normal to γ and κ its mean curvature function. Therefore,

$$\begin{aligned} \frac{\partial}{\partial \gamma} \log \Big(\oint_\gamma K(f - F_{\gamma(s)})ds\Big) &= \frac{\frac{\partial}{\partial \gamma}\oint_\gamma K(f - F_{\gamma(s)})ds}{\oint_\gamma K(f - F_{\gamma(s)})ds} \\ &= \frac{-K(f - F_\gamma)\kappa + \nabla K(f - F_\gamma)\cdot \vec{n}}{\oint_\gamma K(f - F_{\gamma(s)})ds}\, \vec{n} \end{aligned} \tag{9}$$

and $\frac{\partial \mathcal{L}_\gamma}{\partial \gamma} = -\kappa \vec{n}$.
This gives

$$\begin{aligned} \frac{\partial \gamma}{\partial t} &= \frac{\kappa}{\mathcal{L}_\gamma}\vec{n} - \Big[\frac{\kappa}{\mathcal{L}_\gamma}\int_{\mathcal{F}} \frac{\mathcal{M}(f)}{P_\gamma(f)} K(f - F_\gamma)df\Big]\vec{n} \\ &\quad + \frac{\vec{n}}{\mathcal{L}_\gamma}\nabla\Big(\int_{\mathcal{F}} \frac{\mathcal{M}(f)}{P_\gamma(f)} K(f - F_\gamma)df\Big)\cdot \vec{n} \\ &= \frac{1}{\mathcal{L}_\gamma}\Big[\underbrace{\Big(1 - \int_{\mathcal{F}} \frac{\mathcal{M}(f)}{P_\gamma(f)} K(f - F_\gamma)df\Big)\kappa}_{Stopping\ force} \\ &\quad \underbrace{+ \nabla\Big(\int_{\mathcal{F}} \frac{\mathcal{M}(f)}{P_\gamma(f)} K(f - F_\gamma)df\Big)\cdot \vec{n}}_{Refinement\ force}\Big]\vec{n} \end{aligned} \tag{10}$$

which can be written as:

$$\frac{\partial \gamma}{\partial t} = \Bigg(\underbrace{\mathcal{G}_{KL}(P_\gamma, \mathcal{M}, F_\gamma)\kappa}_{Stopping} - \underbrace{\nabla \mathcal{G}_{KL}(P_\gamma, \mathcal{M}, F_\gamma)\cdot \vec{n}}_{refinement}\Bigg)\vec{n}. \tag{11}$$

The evolution equation (11) is of an ordinary geodesic active contour form (Caselles et al., 1997) except that the function $\mathcal{G}_{KL}$ is variable since it depends on the evolving contour, and it references a global information. In general, global information affords added strength to local descriptions in order to ensure stable curve evolution.

When the curve is close to the desired boundary, close to adhering, the curve has a feature density close to the reference density, i.e., $P(F_{\gamma(\mathbf{p})}) \approx M(F_{\gamma(\mathbf{p})})$, which implies that $\mathcal{G}_{KL} \approx 0$. Consequently, the curve behavior is predominantly modulated by the gradient term which drives it to adhere to the desired boundary because it constrains it to move so as to coincide with local highs in the model and curve distributions similarity, just as the common GAC gradient term guides the curve toward local highs in image contrast (Caselles et al., 1997).

3.1 Level Set Implementation

The curve evolution equation is implemented using level set method. The active curve $\gamma(s,t)$ is implicitly

represented by the zero level of a function $\phi(\mathbf{x},t)$: $\Omega \times \mathbb{R}^+ \to \mathbb{R}$, i.e., $\gamma = \{\mathbf{x} \in \Omega \mid \phi(\mathbf{x},t) = 0\}$. Recall (Sethian, 1999) that when γ evolves according to

$$\frac{\partial \gamma(s,t)}{\partial t} = V(s,t)\,\vec{n}(s,t), \tag{12}$$

then ϕ evolves according to

$$\forall \mathbf{x} \in \Omega, \quad \frac{\partial \phi(\mathbf{x},t)}{\partial t} = V(\mathbf{x},t)\|\nabla\phi(\mathbf{x},t)\|, \tag{13}$$

with the convention that $\phi > 0$ inside the zero level-set and $\vec{n}$ is oriented inward. Hence, the level set evolution equation corresponding to the flow (11) is given by

$$V(\mathbf{x},t) = \mathcal{G}(P_\phi, \mathcal{M}, F)\,\kappa_\phi - \nabla\mathcal{G}(P_\phi, \mathcal{M}, F) \cdot \frac{\nabla\phi(\mathbf{x},t)}{\|\nabla\phi(\mathbf{x},t)\|} \tag{14}$$

where $\mathcal{G}$ is $\mathcal{G}_{KL}$. The stopping function is variable of the curve and, therefore, must be updated during evolution using the sample feature distribution within a narrow band δ around the zero level set of ϕ (Sethian, 1999):

$$P_\phi(f) = \frac{\int_{-\delta<\phi(\mathbf{x})<\delta} K(f - F(\mathbf{x}))d\mathbf{x}}{\int_{-\delta<\phi(\mathbf{x})<\delta} d\mathbf{x}}. \tag{15}$$

κ_ϕ is the mean curvature function of ϕ:

$$\kappa_\phi(\mathbf{x},t) = div\left(\frac{\nabla\phi(\mathbf{x},t)}{\|\nabla\phi(\mathbf{x},t)\|}\right), \quad \forall \mathbf{x} \in \Omega \tag{16}$$

Geodesic evolution is often quickened by an additional constant speed c along the curve normal (Caselles et al., 1997), resulting in the level set motion (Li et al., 2005)

$$\frac{\partial \phi(\mathbf{x},t)}{\partial t} = (V(x,t) + c)\|\nabla\phi(\mathbf{x},t)\| \tag{17}$$

4 EXPERIMENTS

In this section we apply the proposed method to various experiments illustrating different applications in order to demonstrate its stated advantages. Indeed, the purpose of this set of experiments is to show that the method can effectively extract, in a single instantiation, all of the regions in an image whose (geometric) feature boundary distribution follows a learned outline pattern. The examples include evaluations over color images from the ETHZ database (Ferrari et al., 2006; Ferrari et al., 2009) and over medical images.

In this set of experiments, we compared the proposed matching functional (abbreviated **CDM** hereafter) to the following functionals:

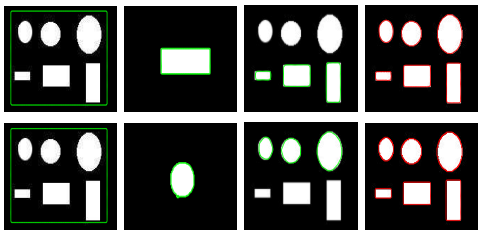

(a) (b) (c) (d)

Figure 2: Detection of regions whose boundaries are consistent with learned outline patterns. Each row depicts a segmentation of the image corresponding to a different model of curvature learned a priori. For example, for the first row the model of curvature is learned independently from the shape of a single rectangle; and for the second row it is learned from a single ellipse with approximately the same aspect ratio as in the figure. Columns: (a) Initial curve positions,(b) training images and contours, (c) the final segmentations, and (d) segmentation with the GAC model (upper) and the RL piece-wise constant model (lower).

RL: The region-based likelihood functional commonly used in image segmentation (Chan and Vese, 2001; Paragios and Deriche, 2002; Rousson and Cremers, 2005; Boykov and Funka Lea, 2006). Optimization of this functional seeks a two-region partition maximizing the conditional probability of pixel data given the learned models within the segmentation regions.

GAC: The classical geodesic active contour functional (Caselles et al., 1997) commonly used in image segmentation as an edge-based constraint, which biases the segmentation boundaries towards high gradients of image data.

GAC-SP: Concatenation of GAC with a shape prior term.

In all the experiments, the feature distribution is estimated using the kernel width $h = 1$ and the narrow band parameter $\delta = 1$.

As stated before, the purpose here is to recover region boundaries consistent with an outline pattern without prior knowledge of the number of regions. Intensity based methods would not allow to do this because, as illustrated in the simple synthetic image of Fig. 2, the targeted regions may have the same intensity distribution as unwanted differently shaped regions. Instead, we will use a geometric feature, namely curvature. Using curvature affords a scheme which handles differences in the pose and number of targeted regions. This is in sharp contrast with shape prior methods which require the knowledge of the number of regions and inclusion of pose parameters in the optimization.

Synthetic Example: Fig. 2 is a synthetic image of

a row of three ellipses of appearances but with approximately the same aspect ratio and a row of different rectangles. The purpose is to segment either all of the rectangular regions, in one instantiation, or all of the ellipsoidal regions but not both. The model curvature (Eq. 4) distributions are learned from one rectangle and one ellipse independently from those appearing in Fig. 2. The contour evolves first towards high contrast boundaries. Once the region boundaries are reached, the proposed CDM flow causes the active curve to remain in coincidence with the desired boundaries but leaves and vanishes from the others. For example, along the boundary of the rectangles (second row), the feature distribution does not match the model distribution of curvature along an ellipse. Therefore, the contour continues to evolve inside the rectangles, and delineates only the elliptical regions at convergence. Evidently, neither region-based segmentation (via RL, for instance) nor edge-based segmentation (via GAC, for instance) will be able to distinguish one type of regions from the other (last column of Fig. 2).

Real Example: The purpose of the second experiment (cf. Fig. 3) is to show the advantage over standard algorithms such as GAC in the case of multiple occurrences of the desired object in a real image. Fig. 3 depicts an example of segmentation of vertebrae in a CT scan of the human spine. The distribution of curvature has been approximated by a histogram along the outline of an exemplar vertebra. Although the results are not totally accurate, CDM (Fig. 3(a)) has been able to segment correctly two vertebrae, do a decent outlining of the others (the poor segmentation of the upper vertebra is due to border effects as no initialization could include this vertebra), and ignore the bone structures on the right. Of course, region-based methods cannot handle this example because the image profile within the vertebrae is very similar to that of other surrounding structures. Edge-based functionals, such as GAC, will bias the active contour to all high image gradients which do not correspond necessarily to the edges of the vertebrae. GAC (Fig. 3(b)) has not been able to do as well on the vertebrae and has included the bone structures on the right.

ETHZ Dataset: In this experiment, we apply the CDM to many images from the ETHZ dataset (Ferrari et al., 2006; Ferrari et al., 2009) in order to test the its efficiency with more complex data. This dataset contains about two hundred images of objects of one of fives types of shapes such as bottles, cups and Apple logos. It has been used to test algorithms which detect and then recognize objects in images. The objects appear in various sizes, positions, colors, and there are within-class variations in shape. The ground truth

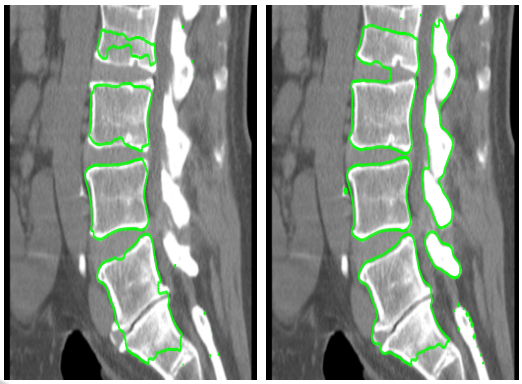

(a) (b)

Figure 3: Segmentation of spine bones in a CT image. (a) final contour position; (b) segmentation with the GAC model.

object shape is provided with each image. Also provided is an edge map obtained by the Berkeley natural boundary detector (Martin et al., 2004; Berg et al., 2005). Although many of the database images are not of use to validate our algorithm, others afford a good test bed. To be of use in our application, an image should, of course, contain several distinct objects to be able to show the detection of the relevant object while ignoring the others. Moreover, the target object should be present in other images, modulo interesting shape variations, to be able to learn a model independently of the test image. Also of use are the images which contain several instances of the relevant object, ideally each modulo a variation in the shape, to show that the algorithm can detect all of the instances. The model distribution is learned on the ground truth of an image different from the test images of the class of objects at hand. Once the model histogram is estimated, the algorithm is run on the edge map rather than the original image. A sample of the obtained results is shown in Fig. 4. The first row contains the test images with the initial curves. The second row contains the edge maps of the images in the the first row. The model curvature histograms are evaluated on the model shapes in the images of the third row. The last row of Fig. 4 shows the position of the evolving curve at convergence. When an object boundary is reached, the distribution matching flow causes the curve to coincide with the desired boundaries but close away from the non desired ones and vanish.

We show now the performance of the a shape based method on two of the tested images where the purpose is to segment all the instances of an object of interest. When the target object occurs more than once in the image, a shape prior will not be able to segment all the instances of that object. Moreover,

Figure 4: A sample of the results on the ETHZ dataset; row 1: initial curve; row 2: edge contours; row 3: shape model; row 4: final curve position.

shape priors generally require pose parameters estimation and, hence, a close initialization is needed which is often impractical. In Fig. 5, we show the results obtained on two different test images using the GAC model with a template matching shape prior term as in (Paragios et al., 2002). For both images, the template used actually corresponds to one of the objects in the image, the smallest ellipse in the first image and the black cup to the right of the second image. Using one of the desired objects as the template simplifies the problem for shape priors because this forgoes the need to optimize with respect to the pose parameters. As expected, the contours evolved towards the objects corresponding to the templates but missed all the other desired object instances.

(a) (b)

Figure 5: Results using the GAC model with a shape prior term: (a,b) final curve positions.

Tracking Example: In this experiment, depicted in Fig. 6, we investigate the tracking of both the left ventricle cavity (first row) and the right ventricle (second

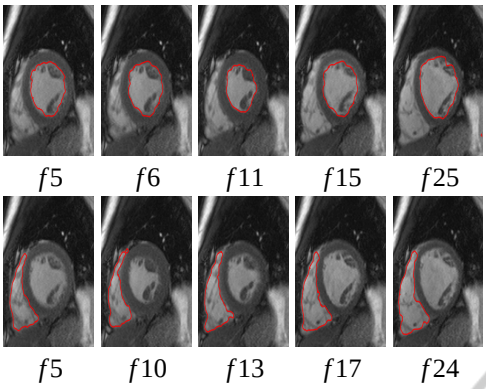

Figure 6: Tracking of both the left ventricle cavity (first row) and the right ventricle (second row) in an MR sequence containing 25 frames (fx depicts frame x). For each frame, the model distributions were learned from the result of the previous frame. The first frame of the sequence was segmented manually.

row) using the curvature as feature. For each frame, the model distributions were learned from the result of the previous frame. The first frame of the sequence was segmented manually. Based on the learned outline pattern, the proposed method succeeds to distinguish between the left and the right ventricles in the considered sequence.

5 CONCLUSIONS

We proposed an active contour edge-based functional which measures the similarity between the curvature distribution on the curve and a learned model distribution. The minimization of the ensuing Euler-Lagrange equation, implemented via level sets, lead to an evolution flow which is viewed as a geodesic active contour with a variable stopping function. This flow drives the active curve until it settles on the boundaries of interest, i.e., boundaries on which the curvature follows the model distribution. The formulation is fundamentally different from region-based schemes which cannot distinguish between regions having the same image distributions. Several experiments confirmed that the proposed method outperforms region and edge based formulations in adverse conditions.

REFERENCES

Ben Ayed, I., Li, S., and Ross, I. (2009). A statistical overlap prior for variational image segmentation. *International Journal of Computer Vision*, 85(1):115–132.

Ben Ayed, I., Mitiche, A., and Belhadj, Z. (2005). Multiregion level set partitioning on synthetic aperture radar images. *IEEE Transactions on Pattern Analysis and Machine Intelligence*, 27(5):793–800.

Ben Ayed, I., Mitiche, A., and Belhadj, Z. (2006). Polarimetric image segmentation via maximum likelihood approximation and efficient multiphase level sets. *IEEE Transactions on Pattern Analysis and Machine Intelligence*, 28(9):1493–1500.

Ben Ayed, I., Mitiche, A., Salah, M. B., and Li, S. (2010). Finding image distributions on active curves. In *CVPR*, pages 3225–3232.

Berg, A., Berg, T., and Malik, J. (2005). Shape matching and object recognition using low distortion correspondance. In *CVPR*.

Boykov, Y. and Funka Lea, G. (2006). Graph cuts and efficient N-D image segmentation. *International Journal of Computer Vision*, 70(2):109–131.

Caselles, V., Kimmel, R., and Sapiro, G. (1997). Geodesic active contours. *International Journal of Computer Vision*, 22(1):61–79.

Chan, T. and Vese, L. (2001). Active contours without edges. *IEEE Transactions on Image Processing*, 10(2):266–277.

Chan, T. and Zhu, W. (2005). Level set based shape prior segmentation. In *Computer Vision and Pattern Recognition*, volume 2, pages 1164–1170.

Cremers, D., Osher, S., and Soatto, S. (2006). Kernel density estimation and intrinsic alignment for shape priors in level set segmentation. *International Journal of Computer Vision*, 69(3):335–351.

Cremers, D., Rousson, M., and Deriche, R. (2007). A review of statistical approaches to level set segmentation: Integrating color, texture, motion and shape. *International Journal of Computer Vision*, 72(2):195–215.

Cremers, D., Sochen, N., and Schnorr, C. (2003). Towards recognition-based variational segmentation using shape priors and dynamic labeling. In *International Conference on Scale Space Theories in Computer Vision*, volume 2695, pages 388–400.

Do Carmo, M. P. (1976). *Differential geometry of curves and surfaces*. Prentice Hall.

Ferrari, V., Jurie, F., and Schmid, C. (2009). From images to shape models for object detection. *International Journal of Computer Vision*.

Ferrari, V., Tuytelaars, T., and Gool, L. V. (2006). Object detection by contour segment networks. In *European Conference on Computer Vision (ECCV),*.

Foulonneau, A., Charbonnier, P., and Heitz, F. (2006). Affine-invariant geometric shape priors for region-based active contours. *IEEE Transactions on Pattern Analysis and Machine Intelligence*, 28(8):1352–1357.

Foulonneau, A., Charbonnier, P., and Heitz, F. (2009). Multi-reference shape priors for active contours. *International Journal of Computer Vision*, 81(1):68–81.

Freedman, D. and Zhang, T. (2004). Active contours for tracking distributions. *IEEE Transactions on Image Processing*, 13(4):518–526.

Holtzman-Gazit, M., Kimmel, R., Peled, N., and Goldsher, D. (2006). Segmentation of thin structures in volumetric medical images. *IEEE Transacions on Image Processing*, 15(2):354–363.

Kass, M., Witkin, A. P., and Terzopoulos, D. (1988). Snakes: Active contour models. *International Journal of Computer Vision*, 1(4):321–331.

Kichenassamy, S., Kumar, A., Olver, P. J., Tannenbaum, A., and Yezzi, A. J. (1995). Gradient flows and geometric active contour models. In *ICCV*, pages 810–815.

Lecellier, F., Jehan-Besson, S., Fadili, J., Aubert, G., and Revenu, M. (2009). Optimization of divergences within the exponential family for image segmentation. In *SSVM*, pages 137–149.

Leventon, M. E., Grimson, W. E., and Faugeras, O. (2000). Statistical shape influence in geodesic active contours. In *Conference on Computer Vision and Pattern Recognition*, volume 1, pages 316–323.

Li, C., Xu, C., Gui, C., and Fox, M. D. (2005). Level set evolution without re-initialization: A new variational formulation. In *Computer Vision and Pattern Recognition*.

Mansouri, A. and Mitiche, A. (2002). Region tracking via local statistics and level set pdes. In *IEEE International Conference on Image Processing*, volume III, pages 605–608, Rochester, NY, USA.

Mansouri, A., Mitiche, A., and Vazquez, C. (2006). Multiregion competition: A level set extension of region competition to multiple region partioning. *Computer Vision and Image Understanding*, 101(3):137–150.

Martin, D., Fowlkes, C., and Malik, J. (2004). Learning to detect natural image boundaries using local brightness, color, and texture cues. *IEEE Transactions on Pattern Analysis and Machine Intelligence*, 26(5):530–549.

Michailovich, O. V., Rathi, Y., and Tannenbaum, A. (2007). Image segmentation using active contours driven by the Bhattacharyya gradient flow. *IEEE Transactions on Image Processing*, 16(11):2787–2801.

Mitiche, A. and Ayed, I. B. (2010). *Variational and Level Set Methods in Image Segmentation*. Springer, 1st edition.

Mortensen, F. N. (2008). *Progress in Autonomous Robot Research*. Nova Science Publishers.

Myronenko, A. and Song, X. B. (2009). Global active contour-based image segmentation via probability alignment. In *CVPR*, pages 2798–2804.

Paragios, N. and Deriche, R. (2002). Geodesic active regions and level set methods for supervised texture segmentation. *International Journal of Computer Vision*, 46(3):223–247.

Paragios, N., Mellina-Gottardo, O., and Ramesh, V. (2004). Gradient vector flow fast geometric active contours. *IEEE Transactions on Pattern Analalysis and Machine Intelligence*, 26(3):402–407.

Paragios, N., Rousson, M., and Ramesh, V. (2002). Matching distance functions: A shape to area variational approach for global to local registration. In *European Conference in Computer Vision (ECCV)*, pages 775–790.

Rousson, M. and Cremers, D. (2005). Efficient kernel density estimation of shape and intensity priors for level set segmentation. In *MICCAI*, pages 757–764.

Salah, M. B., Mitiche, A., and Ayed, I. B. (2010). Effective level set image segmentation with a kernel induced data term. *IEEE Transactions on Image Processing*, 19(1):220–232.

Samson, C., Blanc-Feraud, L., Aubert, G., and Zerubia, J. (2000). A level set model for image classification. *International Journal of Computer Vision*, 40(3):187–197.

Sethian, J. A. (1999). *Level set Methods and Fast Marching Methods*. Cambridge University Press.

Vazquez, C., Mitiche, A., and Laganiere, R. (2006). Joint segmentation and parametric estimation of image motion by curve evolution and level sets. *IEEE Transactions on Pattern Analysis and Machine Intelligence*, 28(5):782–793.

Zhu, S. C. (2003). Statistical modeling and conceptualization of visual patterns. *IEEE Transactions on Pattern Analysis and Machine Intelligence*, 25(6):691–712.

Zhu, S. C. and Yuille, A. (1996). Region competition: Unifying snakes, region growing, and Bayes/MDL for multiband image segmentation. *IEEE Transactions on Pattern Analysis and Machine Intelligence*, 118(9):884–900.